Layered superconductors as nonlinear waveguides for terahertz waves

Sergey Savel'ev,[1,2] V. A. Yampol'skii,[1,3] A. L. Rakhmanov,[1,2,4] and Franco Nori[1,5]
[1]*Frontier Research System, The Institute of Physical and Chemical Research (RIKEN), Wako-shi, Saitama 351-0198, Japan*
[2]*Department of Physics, Loughborough University, Loughborough LE11 3TU, United Kingdom*
[3]*A. Ya. Usikov Institute for Radiophysics and Electronics, Ukrainian Academy of Sciences, 61085 Kharkov, Ukraine*
[4]*Institute for Theoretical and Applied Electrodynamics, Russian Academy of Sciences, 125412 Moscow, Russia*
[5]*Center for Theoretical Physics, CSCS, Department of Physics, University of Michigan, Ann Arbor, Michigan 48109-1040, USA*
(Received 16 October 2006; revised manuscript received 26 December 2006; published 2 May 2007)

We show that unusual nonlinear self-sustained waves, called nonlinear waveguide modes (NWGMs), can propagate along thin slabs of layered superconductors. We show that these waves are stable in the main approximation for extremely anisotropic superconductors if the nonlinear wave amplitude is smaller than a critical value. These modes have no analogs among linear Josephson plasma waves and do not exist in thick samples. The magnetic field of the NWGM is distributed symmetrically with respect to the middle of the slab, decays far from the sample, and can change its sign inside. The impedance ratio of the tangential electric- and magnetic-field amplitudes for NWGMs can be of the order of unity, resulting in a nonmonotonic dispersion relation, $\omega(k)$, strongly sensitive to the NWGM amplitudes. Thus, the "stopping light" phenomenon, now controlled by the magnetic-field amplitude, can be observed. Resonance excitations of the NWGMs should produce anomalies in the amplitude dependence of the reflectivity and transmissivity of the incident terahertz waves, which could be useful for terahertz devices.

DOI: 10.1103/PhysRevB.75.184503 PACS number(s): 74.78.Fk, 74.50.+r

I. INTRODUCTION

Progress in nanotechnology is stimulating intensive studies of electromagnetic waves (EMWs) propagating along artificially fabricated surfaces[1–3] in different media, including metals with modulated properties,[3,4] arrays of coupled waveguides,[5] left-handed materials,[6] and superconductors.[7] The excitation of these waves produces a large variety of resonance anomalies in reflectivity, transmissivity, and absorptivity,[8] offering a new generation of optical nanodevices. Renewed interest in nonlinear surface and waveguide electromagnetic modes (see, e.g., Refs. 1 and 5) is now propelling a new surge of activity in this area.

In this broad context, a layered superconductor is a medium that allows the propagation of both nonlinear[9] *and* surface[7] waves (important for applications[10]) in the terahertz frequency range. Surface waves and nonlinear effects are both due to the gap structure (e.g., Ref. 11) of the Josephson plasma excitation spectra experimentally observed via Josephson plasma resonance (e.g., Ref. 12). The nonlinearity of Josephson plasma waves (JPWs) becomes important even at small magnetic-field amplitudes if EMW frequency ω is lower than the Josephson plasma frequency ω_J and $1-\omega^2/\omega_J^2 \ll 1$. In close analogy to nonlinear optics,[13] nonlinear JPWs exhibit numerous remarkable features,[9] including the slowing down of light, self-focusing effects, and the pumping of weaker waves by stronger ones. However, the nonlinearity of EMWs in layered superconductors is quite different from optical nonlinearities. This leads one to expect very different properties from known nonlinear EMWs.

Here we propose self-sustained JPWs propagating along a thin slab ($-d/2<z<d/2$) of a layered superconductor (both symmetric and antisymmetric with respect to the middle, $z=0$, of the sample). The geometry of the problem considered here is shown in the inset to Fig. 1(b). Weakly nonlinear waves exist in slabs of arbitrary thickness d and coincide with linear surface waves[7] for $d\to\infty$. For *thin* slabs ($d \lesssim \lambda_{ab}$, where λ_{ab} is the in-plane magnetic field penetration depth), essentially nonlinear waveguide modes (NWGMs) are predicted here. Surprisingly, even though the magnetic field H for NWGMs can be very small, the electric field E remains strong. Besides, the magnetic field of the NWGM at the sample surface can be much weaker than the one in the middle of the slab. For this case, the wave amplitude significantly affects the dispersion properties of the NWGMs. The dispersion relation, $\omega(k)$, for this wave mode is nonmonotonic (here, k is the wave vector). As a result, the stop-light phenomenon, $\partial\omega(k,H)/\partial k=0$, controlled by the magnetic-field amplitude H can be observed. We analyze the stability of these waves for very anisotropic superconductors, with anisotropy $\lambda_{ab}/\lambda_c \ll 1$, where λ_c is the out-of-plane penetration depth. We show that the NWGMs are stable if the wave amplitude is smaller than a critical value. The NWGMs predicted here can be experimentally observed via resonance anomalies in the amplitude dependence of the reflectivity and transmissivity of the incident terahertz waves.

II. MODEL

The Maxwell equations for EMWs in vacuum ($z>d/2$) determine the distributions of the magnetic (directed along the y axis) and electric fields,

$$H(x,z>d/2,t) \quad \text{and} \quad E_z(x,z>d/2,t) \propto \exp\{-q_v(z-d/2)\}\cos(kx-\omega t); \tag{1}$$

also,

$$E_x(x,z>d/2,t) \propto \exp\{-q_v(z-d/2)\}\sin(kx-\omega t), \tag{2}$$

with the spatial decrement $q_v=\sqrt{k^2-\omega^2/c^2}$. The impedance ratio,

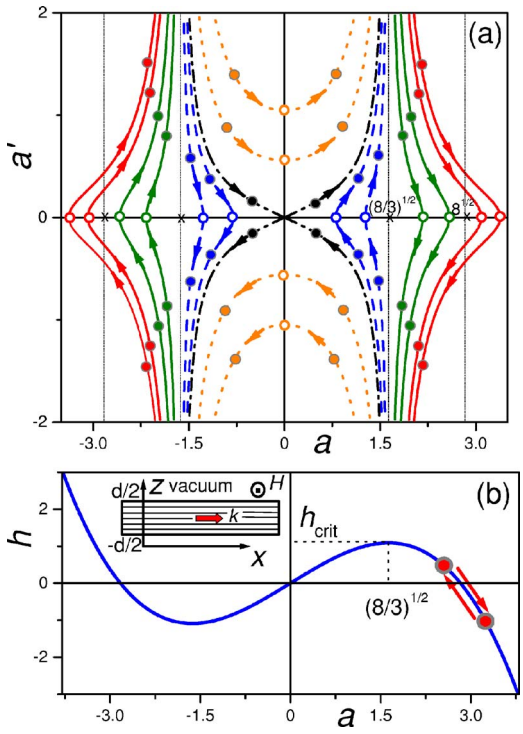

FIG. 1. (Color online) (a) Phase diagram $a'(a)$. Moving along trajectories between solid circles corresponds to the change of coordinate z inside the sample $(-d/2<z<d/2)$. The dashed (blue) and dotted (orange) trajectories mark the symmetric and antisymmetric quasilinear self-sustained modes. The dash-dotted (black) curve separates symmetric and antisymmetric solutions and corresponds to the nonlinear surface wave. The solid trajectories describe the symmetric strongly nonlinear waveguide modes. The solid trajectories correspond to the NWGMs considered in Sec. IV C. (b) The nonmonotonic dependence of the dimensionless magnetic-field amplitude h on the gauge-invariant phase amplitude a according to Eq. (10). The arrows schematically show the change of h and a for the strongly nonlinear waveguide modes inside the sample $(-d/2<z<d/2)$. The inset shows the geometry of the problem.

$$\left.\frac{E_x}{H}\right|_{z=d/2} = -\sqrt{\frac{c^2k^2}{\omega^2}-1}, \tag{3}$$

should match the one obtained for the superconducting slab at the interface $z=d/2$. As for the electromagnetic field at $z<0$, we only consider symmetric and antisymmetric solutions with respect to the middle of the sample $z=0$.

Inside a layered superconductor, the magnetic and electric fields are determined by the gauge-invariant interlayer phase difference φ. We consider nonlinear JPWs with $|\varphi|\ll 1$, where the Josephson current $J_c \sin\varphi$ can be expanded in series as

$$J_c \sin\varphi = J_c\left(\varphi - \frac{\varphi^3}{6} + \frac{\varphi^5}{120} + \cdots\right).$$

In other words, we consider waves, excluding soliton or vortexlike solutions. In the continuum limit, the coupled sine-Gordon equations[14] for the gauge-invariant phase difference φ reduce to

$$\left(1-\lambda_{ab}^2\frac{\partial^2}{\partial z^2}\right)\left[\frac{1}{\omega_J^2}\frac{\partial^2\varphi}{\partial t^2}+\varphi-\frac{\varphi^3}{6}+\frac{\varphi^5}{120}+\cdots\right]-\lambda_c^2\frac{\partial^2\varphi}{\partial x^2}=0. \tag{4}$$

Here we omit the relaxation terms related to the quasiparticle currents. The spatial scales, λ_{ab} and λ_c, are the in-plane and c-axis London penetration depths. As was shown in Ref. 9, the nonlinearity plays a crucial role in wave propagation when

$$(1-\Omega^2)\ll 1, \quad \Omega=\frac{\omega}{\omega_J},$$

since φ^3 is of the same order as $\omega_J^{-2}\partial^2\varphi/\partial t^2+\varphi$, while the higher-order terms, φ^5, can be considered as small corrections. Below we focus on this frequency range.

III. ASYMPTOTIC EXPANSION

We seek a solution of Eq. (4) in the form

$$\varphi(x,z,t)\approx\sum_n A_{2n+1}(z)\sin[(2n+1)(kx-\omega t)]. \tag{5}$$

It is convenient to introduce the dimensionless variables

$$a_{2n+1}=\frac{A_{2n+1}}{(1-\Omega^2)^{1/2}}, \quad \kappa=\frac{\lambda_c k}{(1-\Omega^2)^{1/2}}, \quad \xi=\frac{\kappa z}{\lambda_{ab}}.$$

Beyond the leading order, we derive the equations for the first and third harmonics

$$\left[1-\kappa^2\frac{d^2}{d\xi^2}\right]\left(a_1-\frac{a_1^3}{8}+\frac{1}{8}a_1^2a_3+\frac{1-\Omega^2}{192}a_1^5\right)+\kappa^2a_1=0,$$

$$\left[1-\kappa^2\frac{d^2}{d\xi^2}\right]\left((1-9\Omega^2)a_3+\frac{1-\Omega^2}{24}a_1^3-\frac{1-\Omega^2}{4}a_1^2a_3\right)+9\kappa^2(1-\Omega^2)a_3=0. \tag{6}$$

It follows from these two equations that

$$a_3\sim(1-\Omega^2)a_1\ll a_1. \tag{7}$$

All higher harmonics arise only for higher-order approximations. Similarly, we find that

$$a_{2n+1}\sim(1-\Omega^2)^n a_1. \tag{8}$$

Higher harmonics determine an additional damping mechanism related to the radiation friction of the NWGMs [see the term $\propto a_1^2a_3$ in the first equation of Eq. (6)], which we do not study here.

Therefore, below we restrict our study only to the first harmonic $a_1\equiv a$, which obeys the equation

$$\left[1-\kappa^2\frac{d^2}{d\xi^2}\right]\left(a-\frac{a^3}{8}\right)+\kappa^2a=0, \tag{9}$$

which is correct with an accuracy of about $(1-\Omega^2)/100$.

IV. WAVEGUIDE MODE

For symmetric and antisymmetric solutions, we use the boundary conditions $a'(0)=0$ and $a(0)=0$, respectively, in

the middle of the sample. The electromagnetic fields are related to $a(\xi)$ as follows:

$$H(z) = -H_0(1-\Omega^2)h(\xi)/\kappa,$$

$$h(\xi) = a(\xi) - a^3(\xi)/8,$$

$$E_x(z) = H_0\lambda_{ab}\Omega(1-\Omega^2)h'(\xi)/\sqrt{\epsilon}\lambda_c,$$

$$E_z(z) = H_0\Omega(1-\Omega^2)^{1/2}a(\xi)/\sqrt{\epsilon}. \quad (10)$$

Here, h is a dimensionless magnetic field, prime denotes $d/d\xi$, the scale of the magnetic field is $H_0=\Phi_0/2\pi s\lambda_c$, Φ_0 is the flux quantum, s is the interlayer spacing, and ϵ is the interlayer dielectric constant. The matching of the impedance [continuity of $E_x(z)$ and $H(z)$] at the sample surface $z=d/2$ results in the dispersion relation of the NWGMs:

$$\left(\frac{k^2c^2}{\omega_J^2} - \Omega^2\right)^{1/2} = \frac{\lambda_{ab}}{\sqrt{\epsilon}\lambda_c}\Omega^2\kappa f_s(\Omega,\kappa,H/H_0). \quad (11)$$

The factor

$$f_s = \left.\frac{h'}{h}\right|_{\xi=\kappa d/2\lambda_{ab}} \quad (12)$$

provides the amplitude dependence of the spectrum of the self-sustained waves. This factor has to be obtained by solving Eq. (9). In Eq. (11), we denote $H=H(z=d/2)$.

A. Phase trajectories of self-sustained modes

The decay of the wave in vacuum ($kc>\omega$), which is the necessary condition for waveguide modes, implies the inequality $\kappa \gg 1$ at small $1-\Omega^2$. Since there is no ξ dependence in the coefficients of Eq. (9), we can use the standard substitution $a'=p(a)$ to obtain the first integral. In the limit $\kappa \gg 1$, Eq. (9) yields

$$(a')^2 = -\frac{4}{3} + \frac{G}{(8-3a^2)^2}. \quad (13)$$

The phase diagram of Eq. (13), i.e., the set of $a'(a)$ curves for different constants G, is shown in Fig. 1(a). Different phase trajectories correspond to different types of self-sustained waves in the superconducting slabs. Solid circles mark the sample boundaries, open circles indicate the middle of the slab, and arrows show the direction of motion along the trajectories when ξ increases. In order to match the vacuum-superconductor boundary conditions, the starting and ending points of trajectories should be within the interval from $-\sqrt{8}$ to $\sqrt{8}$. Trajectories confined between $\pm\sqrt{8/3}$ are weak-amplitude modes, called below as quasilinear modes. For these modes, the effective magnetic field h increases with a [Fig. 1(b)] according to Eq. (10). The quasilinear waves can be both symmetric and antisymmetric, and transform to linear surface waves[7] when approaching the point (0,0) in Fig. 1(a). The trajectories with $|a|>\sqrt{8/3}$ represent symmetric strong-amplitude NWGMs with "reverse" dependence $h(a)$ [see Fig. 1(b)], i.e., h decreases when increasing a. This is responsible for the unusual properties of high-amplitude NWGMs: the electric-field amplitude E_z can increase inside the sample, while the magnetic-field amplitude H decreases. There are no strongly nonlinear self-consistent antisymmetric NWGMs.

B. Quasilinear waves

The dashed (blue) and dotted (orange) trajectories in Fig. 1 describe the symmetric and antisymmetric waves having the spectrum in Eq. (11), with

$$f_s = \tanh^m\left(\frac{\kappa d}{\lambda_c}\right)\left(1 + \frac{h_s^2}{32} - m\frac{3h_s^2}{32\cosh^2(\kappa d/\lambda_c)}\right), \quad (14)$$

for $m=1$ and $m=-1$, respectively. Here we assume

$$h_s = h(\xi = \kappa d/2\lambda_{ab}) \ll 1. \quad (15)$$

For thick slabs, $d\to\infty$, the trajectories for both symmetric and antisymmetric waves tend to the dash-dotted trajectory corresponding to the nonlinear surface wave. For $h\to 0$ and $d\to\infty$, the spectrum (14) coincides with the spectrum of linear surface waves obtained in Ref. 7 when ignoring the effect of charge neutrality breaking.[15] Note that the incorporation of charge neutrality breaking has to be done with careful accounting of the so-called additional boundary conditions[16] which could strongly affect the wave spectrum. Here, we neglect this effect, and assume it to be weak, in agreement with experiments.[17]

For the parameters corresponding to the $Bi_2Sr_2CaCu_2O_{8+\delta}$ compounds, the spectrum of symmetric quasilinear waves is located close to the "vacuum light line," $\omega=ck$, and deviates from this line only at very small values of $1-\Omega^2 \sim \lambda_{ab}^2/\epsilon\lambda_c^2$. Thus, these waves are unlikely to be excited in $Bi_2Sr_2CaCu_2O_{8+\delta}$ compounds. However, for artificial superconducting multilayers, or other compounds such as $YBa_2Cu_3O_{7-\delta}$, the conditions for symmetric quasilinear wave excitations could be satisfied.

Concerning the antisymmetric quasilinear waves, their spectrum shifts far from the vacuum light line for thin slabs, $d \ll \lambda_c$ (see Fig. 2). The electromagnetic field of these waves has a very simple, almost linear distribution inside the sample (inset in Fig. 2) and decays in vacuum over a short enough (submillimeter) distance. Due to the latter, layered $Bi_2Sr_2CaCu_2O_{8+\delta}$ superconductors can act as a waveguide for the antisymmetric terahertz modes. Also, nonlinear antisymmetric waves can produce Wood-type anomalies[2] in both amplitude and angular dependence of the reflectivity, transmissivity, and absorptivity coefficients. Similar properties are also inherent for the symmetric strongly nonlinear waves considered below.

C. Symmetric strong-amplitude NWGMs

The function f_s in Eq. (11) describing the deviation of the spectrum of the NWGMs from the vacuum light line has a very complicated structure with asymptotics:

$$f_s \propto \frac{\kappa d}{h_s\lambda_{ab}} \quad \text{for} \quad \frac{\kappa^2 d^2}{\lambda_{ab}^2} \ll 1 - h_s \quad (16)$$

and

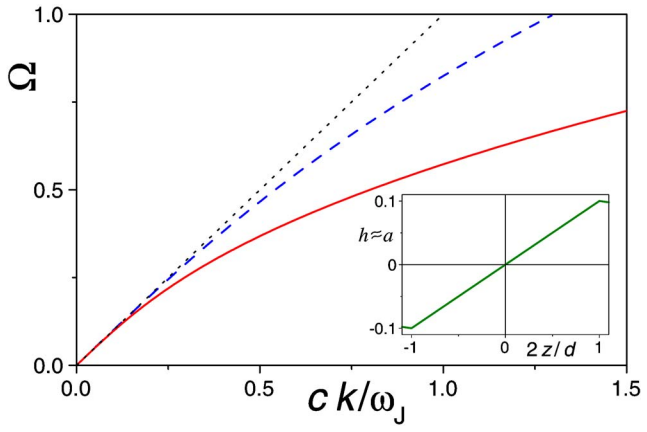

FIG. 2. (Color online) Dispersion relation, $\Omega(ck/\omega_J)$, for the antisymmetric waveguide mode. Parameters are $\lambda_c/\lambda_{ab}=200$, $\varepsilon=16$, and $d/\lambda_{ab}=0.1$ and 0.3 for solid (red) and dashed (blue) curves, respectively. The dotted (black) line corresponds to the "vacuum light line." Inset: schematics of the spatial distribution of the dimensionless magnetic-field amplitude $h(2z/d)\approx a(2z/d)$ inside the sample.

$$f_s \propto \frac{\kappa^2 d^2}{h_s \lambda_{ab}^2} \quad \text{for} \quad \frac{\kappa d}{\lambda_{ab}} \gg 1. \tag{17}$$

This allows one to construct a simple interpolation of the dispersion relation

$$1-\Omega^2 = \frac{d^2}{3\epsilon\lambda_{ab}^2}\left[\left(\frac{H}{H_t}\right)^2\left(1-\frac{\omega_J^2}{c^2k^2}\right)-\frac{c^2k^2}{4\omega_J^2}\right], \tag{18}$$

where the threshold amplitude

$$H_t \approx \frac{0.8H_0d^2}{\epsilon^{3/2}\lambda_{ab}\lambda_c} \tag{19}$$

defines the lowest value of the magnetic-field amplitude at the sample surface: at lower fields, the predicted NWGMs do not exist. The interpolation formula Eq. (18) is in perfect agreement with numerical results (see Fig. 3) obtained by the integration of Eq. (13).

The spectrum of the strong-amplitude NWGMs is nonmonotonic (Fig. 3) and $\Omega(k)$ reaches the minimal value

$$\Omega_{\min} = \left\{1-\frac{d^2H}{3\epsilon\lambda_{ab}^2H_t}\left(\frac{H}{H_t}-1\right)\right\}^{1/2} \tag{20}$$

at

$$k = \frac{\omega_J}{c}\sqrt{\frac{2H}{H_t}}. \tag{21}$$

Thus, the stop-light phenomenon, $\partial\omega(k,H)/\partial k=0$, occurs in the terahertz superconducting waveguide. This stop-light effect can be easily controlled by the magnetic-field amplitude.

It is interesting to note that the spectrum of the NWGMs is located between (k_s,Ω_s) and (k_f,Ω_f). At these peculiar points of the spectrum, the value of the dimensionless magnetic-field amplitude h achieves its critical value

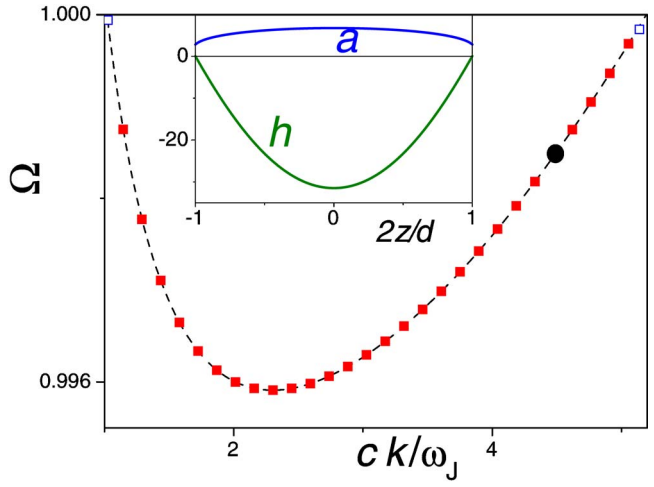

FIG. 3. (Color online) Dispersion relation, $\Omega(ck/\omega_J)$, for the strongly nonlinear waveguide mode: the solid squares present the result of the numerical simulation using Eq. (13); the dashed line is obtained by interpolating between two asymptotics. The simulations and interpolation perfectly coincide. Here we use the following set of parameters: $d/\lambda_{ab}=0.3$, $\lambda_c/\lambda_{ab}=200$, $\varepsilon=16$, and $H/H_0=1.5\times10^{-5}$. Inset: the spatial distribution of the dimensionless magnetic-field amplitude $h(2z/d)$ and the amplitude of the gauge-invariant phase difference $a(2z/d)$ inside the sample, for the same set of parameters as in the main panel and for Ω and ck/ω_J marked by the solid circle in the main panel. Open squares mark the starting and ending points of the spectrum.

$$h_{\text{crit}} = h(a=\sqrt{8/3}) = \sqrt{32/27} \tag{22}$$

[see Fig. 1(b)]. At the sample edges $z=d/2$, a' tends to infinity according to Eq. (13), but h' is not singular.

For the strong-amplitude NWGMs, the magnetic-field amplitude at the sample surface is less than inside the slab, while the phase $a(\xi)$ and, thus, the electric field E_z do not significantly change in the sample (see inset of Fig. 3). Due to this feature, e.g., $H(0)/H(d/2)\gg1$, the spectrum of the NWGMs is remarkably far from the $\omega=ck$ line despite the smallness of the parameter $\lambda_{ab}/\sqrt{\epsilon}\lambda_c$ in Eq. (11).

The numerical analysis of Eqs. (9) and (11) [or Eq. (18)] shows that strong-amplitude NWGMs exist for sample thicknesses d smaller than some critical value d_c because of the instability of NWGMs for thick samples (see the next section). This threshold thickness d_c depends on the sample parameters (in particular, $\gamma=\lambda_c/\lambda_{ab}$ and ε) as well as the NWGM frequency and wave vector. However, d_c is about several λ_{ab} in any realistic case. For given parameters of the incident EMW and material characteristics (e.g., γ and ε), the amplitude of the magnetic field and the gauge-invariant phase oscillations increase in the middle of the sample when the sample thickness d grows. When $d>d_c$, the large-amplitude NWGMs suddenly become unstable. However, the large-amplitude NWGMs are stable with respect to small perturbations when d is smaller than d_c.

V. STABILITY OF STRONG-AMPLITUDE WAVEGUIDE MODES

To study the stability of NWGMs with respect to small perturbations, we seek a solution of Eq. (4) in the form

$$\varphi = a\sqrt{1-\Omega^2}\sin(\kappa\zeta-\omega t)+\exp(iq\zeta+\Lambda\omega_J t)\times[\alpha(\xi)\sin(\kappa\zeta-\omega t)+\beta(\xi)\cos(\kappa\zeta-\omega t)], \quad (23)$$

where

$$\zeta = \frac{x\sqrt{1-\Omega^2}}{\lambda_c}. \quad (24)$$

Here, the first term is the solution corresponding to the strong-amplitude NWGM studied above. The other two terms are small fluctuations that could result in a modulating instability. A positive $\Re e(\Lambda)$ would produce a modulational instability with wave vector q. The fluctuations can be symmetric,

$$\alpha(\xi)=\alpha\cosh(p\xi), \quad \beta(\xi)=\beta\cosh(p\xi), \quad (25)$$

or antisymmetric,

$$\alpha(\xi)=\alpha\sinh(p\xi), \quad \beta(\xi)=\beta\sinh(p\xi), \quad (26)$$

with respect to the middle of the sample, $\xi=0$. Following the approach presented in Sec. III, we now keep only the first harmonics of the cubic term in the coupled sine-Gordon equation (4).

For simplicity, we neglect the coordinate dependence of the nonlinear wave amplitude $a(\xi)$. Indeed, the NWGM amplitude is almost constant across the sample cross section, as seen in the inset of Fig. 3. Substituting Eq. (23) into the coupled sine-Gordon equation (4), we obtain a set of linear homogeneous algebraic equations for the constants α and β, which are the same for both symmetric and antisymmetric solutions,

$$\alpha\{(1-\kappa^2p^2)[1-3a^2/8+\Lambda^2/(1-\Omega^2)]+q^2+\kappa^2\}+2\beta[(1-\kappa^2p^2)\Lambda\Omega/(1-\Omega^2)+iq\kappa]=0,$$

$$2\alpha[(1-\kappa^2p^2)\Lambda\Omega/(1-\Omega^2)+iq\kappa]-\beta\{(1-\kappa^2p^2)\times[1-a^2/8+\Lambda^2/(1-\Omega^2)]+q^2+\kappa^2\}=0. \quad (27)$$

Nontrivial solutions for α and β exist if the determinant of the system of Eqs. (27) is zero. This results in

$$4[(1-\kappa^2p^2)\Lambda\Omega/(1-\Omega^2)+iq\kappa]^2+\{(1-\kappa^2p^2)\times[1-a^2/8+\Lambda^2/(1-\Omega^2)]+q^2+\kappa^2\}\times\{(1-\kappa^2p^2)(1-3a^2/8+\Lambda^2/(1-\Omega^2)]+q^2+\kappa^2\}=0. \quad (28)$$

The fluctuating field is the sum of two terms corresponding to two solutions, p_1 and p_2, for p in Eq. (28). We now analyze the symmetric fluctuations only,

$$\alpha(\xi)=\alpha_1\cosh(p_1\xi)+\alpha_2\cosh(p_2\xi), \quad \beta(\xi)=\beta_1\cosh(p_1\xi)+\beta_2\cosh(p_2\xi). \quad (29)$$

The analysis of the antisymmetric fluctuations (in the limit $\lambda_{ab}/\lambda_c\to 0$) is similar and leads to the same results.

Matching the impedance at the sample boundary, we derive the long equations (A13) and (A14) for the coefficients α and β specified in the Appendix. However, these equations contain a very small parameter $\lambda_{ab}/\lambda_c \ll 1$, which is about 1/500 for Bi2212. In the leading approximation with respect to this parameter, Eqs. (A13) and (A14) are reduced to

$$U\left[1-\frac{3a^2}{8}-\frac{2i\Omega\Lambda}{1-\Omega^2}+\frac{\Lambda^2}{1-\Omega^2}\right]+iV\left[1-\frac{a^2}{8}-\frac{2i\Omega\Lambda}{1-\Omega^2}+\frac{\Lambda^2}{1-\Omega^2}\right]=0,$$

$$U\left[1-\frac{3a^2}{8}+\frac{2i\Omega\Lambda}{1-\Omega^2}+\frac{\Lambda^2}{1-\Omega^2}\right]-iV\left[1-\frac{a^2}{8}+\frac{2i\Omega\Lambda}{1-\Omega^2}+\frac{\Lambda^2}{1-\Omega^2}\right]=0, \quad (30)$$

with

$$U=\alpha_1\cosh(p_1\xi_d)+\alpha_2\cosh(p_2\xi_d), \quad V=\beta_1\cosh(p_1\xi_d)+\beta_2\cosh(p_2\xi_d).$$

Equating the determinant of this set of equations to zero, we obtain the dispersion relation for the increment Λ,

$$\Lambda^4+\Lambda^2\left[4\Omega^2+\left(2-\frac{a^2}{2}\right)(1-\Omega^2)\right]+1-\frac{a^2}{2}+\frac{3a^4}{64}=0. \quad (31)$$

Since $1-\Omega^2\ll 1$ and $(1-a^2/2+3a^4/64)>0$ for $a^2>8/3$, we conclude that the roots of this equation are purely imaginary for NWGM amplitudes if $a<a_c\approx 3.87$. At higher amplitudes, $a>a_c$, the roots with nonzero real part appear and two of them have positive real parts. The numerical solution of Eqs. (9) and (11) shows that the wave amplitude a is significantly higher than the critical value a_c if the sample thickness is close to its maximum value d_c.

Near the critical amplitude a_c, the instability increment Λ can be written as

$$\Lambda=\left(\frac{a^2-a_c^2}{32}\right)^{1/2}\pm i\sqrt{2}. \quad (32)$$

For the trivial solution of Eqs. (30), we obtain

$$\frac{\alpha_1}{\alpha_2}=\frac{\beta_1}{\beta_2}=-\frac{\cosh(p_2\xi_d)}{\cosh(p_1\xi_d)}. \quad (33)$$

Using Eqs. (28) and (A1), we derive a quadratic equation for Λ

$$\Lambda^2+i\Lambda\frac{\Omega(q^2+\kappa^2)}{q\kappa}+\left(1-\frac{3a^2}{8}\right)(1-\Omega^2)=0. \quad (34)$$

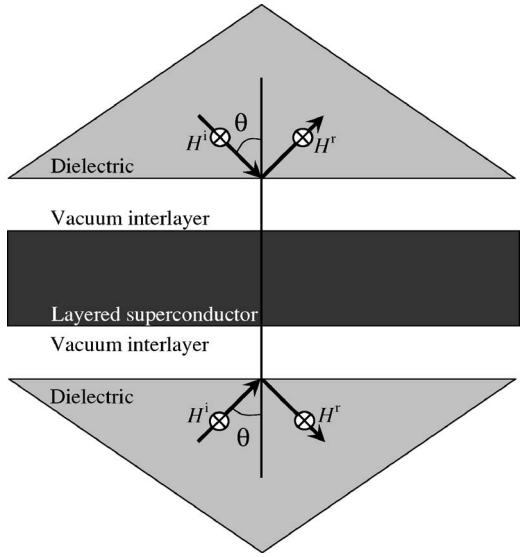

FIG. 4. A proposed geometry for an experiment probing the resonance excitations of NWGMs in a layered superconductor sandwiched between two dielectric prisms.

Both roots of this equation are imaginary.

Thus, in the main approximation with respect to the small parameter $\lambda_{ab}/\lambda_c \ll 1$, the increments Λ are imaginary and the NWGMs considered are stable at low amplitudes when $a < a_c$. Otherwise, a modulating instability can develop.

VI. ANOMALIES IN THE AMPLITUDE DEPENDENCE OF THE REFLECTION COEFFICIENTS DUE TO THE RESONANCE EXCITATION OF THE NONLINEAR WAVEGUIDE MODES

In this section, we show that nonlinear waveguide modes can be excited in a superconducting slab using two dielectric prisms. As a result of the NWGM excitation, a resonance increase of the electromagnetic absorptivity can be observed if the ac amplitude, frequency, and wave vector satisfy the dispersion relation, Eq. (18). Let us now consider the p (TM)-polarized plane monochromatic electromagnetic wave incident from the dielectric prisms through the vacuum interlayers onto a plate of layered superconductor, from both of its sides (see Fig. 4). This experimental configuration corresponds to the so-called prism method of excitation of surface waves (also known as Otto configuration[18,19]) with attenuated total wave reflection. Usually, the incident angle θ is varied in one-sided or unilateral experiments, and the resonance suppression of the wave reflection is observed if the wave vector $k_x = (\sqrt{\varepsilon}\omega/c)\sin(\theta)$ satisfies the dispersion relation for the surface wave in a conductor. Here ε is the dielectric constant of the prisms.

Two essential additional features of this proposed experiment are important for our case. First, the superconducting plate is excited on both sides, resulting in the magnetic field of the incident waves symmetric with respect to the middle of the superconducting plate. Second, the considered waveguide mode is nonlinear. This offers a possibility to observe the anomalies in the reflection coefficient and absorptivity as a function of the *amplitude* of the incident wave with given frequency and incident angle. This allows one to distinguish the predicted nonlinear waveguide modes from linear ones (for which there is no amplitude anomaly). Namely, if the sum of the magnetic fields of the incident and reflected waves at the sample surfaces takes the resonance value $H_{\rm res}$,

$$H_{\rm res} = H_t \left\{ \frac{\sin^2(\theta)\varepsilon}{\sin^2(\theta)\varepsilon - 1} \left[\frac{3\epsilon\lambda_{ab}^2(1-\Omega^2)}{d^2} + \frac{\sin^2(\theta)\varepsilon}{4} \right] \right\}^{1/2} \tag{35}$$

and

$$\sin^2(\theta) > \frac{1}{\varepsilon}, \tag{36}$$

a sharp decrease of the reflection coefficient and increase of the electromagnetic absorption should be observed.

VII. CONCLUSIONS

The dependence of the dispersion relation on the wave amplitude is the main feature that can be used to experimentally distinguish the predicted NWGMs from ordinary plasma waves. The excitation of NWGMs produces an increase in the EMW absorption by the sample near the plasma frequency if the amplitude of the incident wave H exceeds the threshold value H_t [Eq. (19)]. Using characteristic values for BSCCO ($\lambda_{ab}=200$ nm, $\gamma=200$, $\varepsilon=20$, and $s=15$ nm) and assuming that the sample thickness d is equal to λ_{ab}, we obtain $H_t \approx 2\times 10^{-3}$ Oe, which corresponds to a power of the incident (from the vacuum) EMWs of the order of 1 mW/cm^2.

Thus, we predict the existence of both strongly nonlinear symmetric and weakly nonlinear antisymmetric waveguide modes, which propagate in a thin slab of layered superconductors and decay fast enough in the vacuum. The spectrum of strongly nonlinear symmetric waveguide modes is nonmonotonic, resulting in a "stop-light" effect controlled by the magnetic-field intensity. These nonlinear self-sustained waveguide modes could be observed via amplitude and angular anomalies in the reflectivity and absorptivity of incident terahertz electromagnetic waves. The predicted terahertz modes could be potentially useful for the design of terahertz waveguides, detectors, and filters.[20]

ACKNOWLEDGMENTS

We gratefully acknowledge partial support from the National Security Agency (NSA), Laboratory Physical Science (LPS), Army Research Office (ARO), National Science Foundation (NSF) Grant No. EIA-0130383, No. JSPS-RFBR 06-02-91200, and Core-to-Core (CTC) program supported by the Japan Society for Promotion of Science (JSPS). S.S. acknowledges support from the Ministry of Science, Culture and Sports of Japan via the Grant-in Aid for Young Scientists Grant No. 18740224, the EPSRC Advanced Research Grant No. EP/D072581/1, and ESF network program "Arrays of Quantum Dots and Josephson Junctions."

APPENDIX: MATCHING IMPEDANCE FOR THE FLUCTUATING FIELDS

Here we derive equations for the small perturbation amplitudes that could result in a modulation instability. According to Eqs. (27), the values β_1 and β_2 are related to α_1 and α_2 as

$$\beta_i = 2\alpha_i \frac{(1-\kappa^2 p_i^2)\Lambda\Omega/(1-\Omega^2) + iq\kappa}{(1-\kappa^2 p_i^2)[1-a^2/8+\Lambda^2/(1-\Omega^2)]+q^2+\kappa^2}. \tag{A1}$$

Expressions for α_1 and α_2, as well as the dispersion equation for the instability increment Λ, can be derived by matching the tangential components of the electric and magnetic fields at the sample boundary $z=d/2$ ($\xi=\xi_d=\kappa d/2\lambda_{ab}$). These components are expressed, via the phase difference φ, as

$$E_x = \frac{\lambda_{ab}}{c}\kappa\frac{\partial^2 H}{\partial\xi\partial t}, \quad \frac{\partial H}{\partial\zeta} = \frac{H_0}{\sqrt{1-\Omega^2}}\left(\varphi - \frac{\varphi^3}{6} - \frac{1}{\omega_J^2}\frac{\partial^2\varphi}{\partial t^2}\right). \tag{A2}$$

Using Eqs. (23) and (A2), we derive the equations for the magnetic and electric fields inside the sample

$$H_s = H_1(\xi)\exp[i(q+\kappa)\zeta + \Lambda t - i\omega_J t] + H_2(\xi)\exp[i(q-\kappa)\zeta + \Lambda t + i\omega_J t], \tag{A3}$$

$$E_{sx} = E_{x1}(\xi)\exp[i(q+\kappa)\zeta + \Lambda t - i\omega_J t] + E_{x2}(\xi)\exp[i(q-\kappa)\zeta + \Lambda t + i\omega_J t], \tag{A4}$$

where the field amplitudes are

$$H_1(\xi) = -\frac{H_0\sqrt{1-\Omega^2}}{2(q+\kappa)}\left\{\alpha(\xi)\left(1-\frac{3a^2}{8}+\frac{\Lambda^2}{1-\Omega^2}-\frac{2i\Omega\Lambda}{1-\Omega^2}\right) + i\beta(\xi)\left(1-\frac{a^2}{8}+\frac{\Lambda^2}{1-\Omega^2}-\frac{2i\Omega\Lambda}{1-\Omega^2}\right)\right\}, \tag{A5}$$

$$H_2(\xi) = \frac{H_0\sqrt{1-\Omega^2}}{2(q-\kappa)}\left\{\alpha(\xi)\left(1-\frac{3a^2}{8}+\frac{\Lambda^2}{1-\Omega^2}+\frac{2i\Omega\Lambda}{1-\Omega^2}\right) - i\beta(\xi)\left(1-\frac{a^2}{8}+\frac{\Lambda^2}{1-\Omega^2}+\frac{2i\Omega\Lambda}{1-\Omega^2}\right)\right\}, \tag{A6}$$

$$E_{x1}(\xi) = -\frac{H_0\lambda_{ab}\kappa\sqrt{1-\Omega^2}}{2c(q+\kappa)}(\Lambda\omega_J - i\omega) \times\left\{\alpha'(\xi)\left(1-\frac{3a^2}{8}+\frac{\Lambda^2}{1-\Omega^2}-\frac{2i\Omega\Lambda}{1-\Omega^2}\right) + i\beta'(\xi) \times\left(1-\frac{a^2}{8}+\frac{\Lambda^2}{1-\Omega^2}-\frac{2i\Omega\Lambda}{1-\Omega^2}\right)\right\}, \tag{A7}$$

$$E_{x2}(\xi) = -\frac{H_0\lambda_{ab}\kappa\sqrt{1-\Omega^2}}{2c(q-\kappa)}(\Lambda\omega_J + i\omega) \times\left\{-\alpha'(\xi)\left(1-\frac{3a^2}{8}+\frac{\Lambda^2}{1-\Omega^2}+\frac{2i\Omega\Lambda}{1-\Omega^2}\right) + i\beta'(\xi) \times\left(1-\frac{a^2}{8}+\frac{\Lambda^2}{1-\Omega^2}+\frac{2i\Omega\Lambda}{1-\Omega^2}\right)\right\}. \tag{A8}$$

In vacuum at $z>d/2$, the fluctuations of the magnetic and electric fields can be written as

$$H_v = H_{v1}\exp[i(q+\kappa)\zeta + \Lambda t - i\omega_J t]\exp(iK_1 z) + H_{v2}\exp(i[q-\kappa)\zeta + \Lambda t + i\omega_J t]\exp(iK_2 z), \tag{A9}$$

$$E_{xv} = E_{xv1}\exp[i(q+\kappa)\zeta + \Lambda t - i\omega_J t]\exp(iK_1 z) + E_{xv2}\exp[i(q-\kappa)\zeta + \Lambda t + i\omega_J t]\exp(iK_2 z). \tag{A10}$$

The Maxwell equations yield the connections between the field amplitudes and the dispersion relation for the z components of the wave vectors K_i in vacuum,

$$E_{xv1} = -H_{v1}\frac{icK_1}{\Lambda - i\omega}, \quad E_{xv2} = -H_{v2}\frac{icK_2}{\Lambda + i\omega}, \tag{A11}$$

$$K_1 = \sqrt{\frac{(\omega + i\Lambda\omega_J)^2}{c^2} - (q+\kappa)^2\frac{1-\Omega^2}{\lambda_c^2}},$$

$$K_2 = \sqrt{\frac{(\omega - i\Lambda\omega_J)^2}{c^2} - (q-\kappa)^2\frac{1-\Omega^2}{\lambda_c^2}}, \quad \mathrm{Im}\, K_i > 0. \tag{A12}$$

Substituting Eq. (29) into Eqs. (A5)–(A10) and matching the electric and magnetic fields at the boundary, $z=d/2$, separately for terms proportional to $\exp[i(q\pm\kappa)\zeta + \Lambda t \mp i\omega_J t]$, we find two linear equations for constants α_i and β_i

$$\frac{\kappa\lambda_{ab}}{\lambda_c\sqrt{\varepsilon}}(\Lambda - i\Omega)\Bigg\{[p_1\alpha_1 \sinh(p_1\xi_d) + p_2\alpha_2 \sinh(p_2\xi_d)] \times\left[1 - \frac{3a^2}{8} - \frac{2i\Omega\Lambda}{1-\Omega^2} + \frac{\Lambda^2}{1-\Omega^2}\right] + i[p_1\beta_1 \sinh(p_1\xi_d) + p_2\beta_2 \sinh(p_2\xi_d)]\left[1 - \frac{a^2}{8} - \frac{2i\Omega\Lambda}{1-\Omega^2} + \frac{\Lambda^2}{1-\Omega^2}\right]\Bigg\}$$
$$= i\sqrt{\frac{\varepsilon(q+\kappa)^2(1-\Omega^2)}{(\Omega+i\Lambda)^2} - 1}\Bigg\{[\alpha_1 \cosh(p_1\xi_d) + \alpha_2 \cosh(p_2\xi_d)]\left[1 - \frac{3a^2}{8} - \frac{2i\Omega\Lambda}{1-\Omega^2} + \frac{\Lambda^2}{1-\Omega^2}\right] + i[\beta_1 \cosh(p_1\xi_d) + \beta_2 \cosh(p_2\xi_d)]\left[1 - \frac{a^2}{8} - \frac{2i\Omega\Lambda}{1-\Omega^2} + \frac{\Lambda^2}{1-\Omega^2}\right]\Bigg\}, \tag{A13}$$

$$\frac{\kappa\lambda_{ab}}{\lambda_c\sqrt{\varepsilon}}(\Lambda + i\Omega)\Bigg\{[p_1\alpha_1 \sinh(p_1\xi_d) + p_2\alpha_2 \sinh(p_2\xi_d)] \times\left[1 - \frac{3a^2}{8} + \frac{2i\Omega\Lambda}{1-\Omega^2} + \frac{\Lambda^2}{1-\Omega^2}\right] - i[p_1\beta_1 \sinh(p_1\xi_d) + p_2\beta_2 \sinh(p_2\xi_d)]\left[1 - \frac{a^2}{8} + \frac{2i\Omega\Lambda}{1-\Omega^2} + \frac{\Lambda^2}{1-\Omega^2}\right]\Bigg\}$$
$$= i\sqrt{\frac{\varepsilon(q-\kappa)^2(1-\Omega^2)}{(\Omega-i\Lambda)^2} - 1}\Bigg\{[\alpha_1 \cosh(p_1\xi_d) + \alpha_2 \cosh(p_2\xi_d)]\left[1 - \frac{3a^2}{8} + \frac{2i\Omega\Lambda}{1-\Omega^2} + \frac{\Lambda^2}{1-\Omega^2}\right] + i[\beta_1 \cosh(p_1\xi_d) + \beta_2 \cosh(p_2\xi_d)]\left[1 - \frac{a^2}{8} + \frac{2i\Omega\Lambda}{1-\Omega^2} + \frac{\Lambda^2}{1-\Omega^2}\right]\Bigg\}. \tag{A14}$$

In the limit $\lambda_{ab}/\lambda_c \to 0$, we derive Eq. (30) presented in the text.

[1] D. N. Christodoulides, F. Lederer, and Ya. Silberger, Nature (London) **424**, 817 (2003).

[2] B. Barnes and R. Sambles, Phys. World **19** (1), 17 (2006); Th. Krauss, *ibid.* **19** (2), 32 (2006).

[3] T. W. Ebbesen, H. J. Lezec, H. F. Ghaemi, T. Thio, and P. A. Wolff, Nature (London) **391**, 667 (1998); R. Gordon, A. G. Brolo, A. McKinnon, A. Rajora, B. Leathem, and K. L. Kavanagh, Phys. Rev. Lett. **92**, 037401 (2004).

[4] A. V. Kats, M. L. Nesterov, and A. Yu. Nikitin, Phys. Rev. B **72**, 193405 (2005); A. V. Kats and I. S. Spevak, *ibid.* **65**, 195406 (2002); A. V. Kats, S. Savel'ev, V. A. Yampol'skii, and F. Nori, Phys. Rev. Lett. **98**, 073901 (2007).

[5] S. Suntsov, K. G. Makris, D. N. Christodoulides, G. I. Stegeman, A. Haché, R. Morandotti, H. Yang, G. Salamo, and M. Sorel, Phys. Rev. Lett. **96**, 063901 (2006).

[6] R. Ruppin, J. Phys.: Condens. Matter **13**, 1811 (2001); I. V. Shadrivov, A. A. Sukhorukov, and Yu. S. Kivshar, Phys. Rev. E **67**, 057602 (2003).

[7] S. Savel'ev, V. Yampol'skii, and F. Nori, Phys. Rev. Lett. **95**, 187002 (2005); Physica C **445-448**, 183 (2006).

[8] A. Hessel and A. A. Oliner, Appl. Opt. **4**, 1275 (1965); H. Raether, *Surface Plasmons* (Springer, New York, 1988); R. Petit, *Electromagnetic Theory of Gratings* (Springer, Berlin, 1980).

[9] S. Savel'ev, A. Rakhmanov, V. Yampol'skii, and F. Nori, Nat. Phys. **2**, 521 (2006).

[10] See, e.g., the special issue in Philos. Trans. R. Soc. London, Ser. A **362**, (1815) (2004).

[11] T. M. Mishonov, Phys. Rev. B **44**, 12033 (1991); L. N. Bulaevskii, M. P. Maley, and M. Tachiki, Phys. Rev. Lett. **74**, 801 (1995).

[12] Y. Matsuda, M. B. Gaifullin, K. Kumagai, K. Kadowaki, and T. Mochiku, Phys. Rev. Lett. **75**, 4512 (1995).

[13] D. L. Mills, *Nonlinear Optics* (Springer, Berlin, 1998); N. Bloembergen, *Nonlinear Optics* (World Scientific, Singapore, 1996); Y. R. Shen, *The Principles of Nonlinear Optics* (Wiley-Interscience, Hoboken, NJ, 2003).

[14] S. Sakai, P. Bodin, and N. F. Pedersen, J. Appl. Phys. **73**, 2411 (1993); M. Tachiki and M. Machida, Physica C **341-348**, 1493 (2000); S. N. Artemenko and S. V. Remizov, *ibid.* **362**, 200 (2001).

[15] M. Machida, T. Koyama, and M. Tachiki, Phys. Rev. Lett. **83**, 4618 (1999).

[16] C. Helm, L. N. Bulaevskii, E. M. Chudnovsky, and M. P. Maley, Phys. Rev. Lett. **89**, 057003 (2002); C. Helm and L. N. Bulaevskii, Phys. Rev. B **66**, 094514 (2002).

[17] S. Rother, Y. Koval, P. Müller, R. Kleiner, D. A. Ryndyk, J. Keller, and C. Helm, Phys. Rev. B **67**, 024510 (2003).

[18] A. Otto, Z. Phys. **216**, 398 (1968).

[19] A. Otto, in *Polaritons*, Proceedings of the First Taormina Conference on the Structure of Matter (Pergamon, New York, 1974), p. 117.

[20] S. Savel'ev, A. L. Rakhmanov, and F. Nori, Phys. Rev. Lett. **94**, 157004 (2005); Physica C **445-448**, 180 (2006); S. Savel'ev, V. Yampol'skii, A. Rakhmanov, and F. Nori, Phys. Rev. B **72**, 144515 (2005); Physica C **437-438**, 281 (2006); **445-448**, 175 (2006); V. A. Yampol'skii, S. Savel'ev, O. V. Usatenko, S. S. Mel'nik, F. V. Kusmartsev, A. A. Krokhin, and F. Nori, Phys. Rev. B **75**, 014527 (2007); S. Savel'ev, A. L. Rakhmanov, and F. Nori, Phys. Rev. Lett. **98**, 077002 (2007).